

Photoemission and DMFT study of electronic correlations in SrMoO₃: Effects of Hund's rule coupling and possible plasmonic sideband

H. Wadati,^{1,*} J. Mravlje,^{2,3,4} K. Yoshimatsu,⁵ H. Kumigashira,⁵ M. Oshima,⁵ T. Sugiyama,⁶ E. Ikenaga,⁶ A. Fujimori,⁷ A. Georges,^{3,4,8} A. Radetinac,⁹ K. S. Takahashi,¹⁰ M. Kawasaki,^{1,10} and Y. Tokura^{1,10}

¹*Department of Applied Physics and Quantum-Phase Electronics Center (QPEC), University of Tokyo, Hongo, Tokyo 113-8656, Japan*

²*Jozef Stefan Institute, Jamova 39, Ljubljana, Slovenia*

³*Collège de France, 11 place Marcelin Berthelot, 75005 Paris, France*

⁴*Centre de Physique Théorique, École Polytechnique, CNRS, 91128 Palaiseau, France*

⁵*Department of Applied Chemistry, University of Tokyo, Bunkyo-ku, Tokyo 113-8656, Japan*

⁶*Japan Synchrotron Radiation Research Institute, SPring-8, Hyogo 679-5198, Japan*

⁷*Department of Physics, University of Tokyo, Bunkyo-ku, Tokyo 113-0033, Japan*

⁸*DPMC, Université de Genève, 24 quai Ernest-Ansermet, 1211 Genève 4, Switzerland*

⁹*Institut für Materialwissenschaft, Technische Universität Darmstadt, Petersenstrabe 23, 64287 Darmstadt, Germany*

¹⁰*RIKEN Center for Emergent Matter Science (CEMS), Wako 351-0198, Japan*

(Received 20 August 2013; revised manuscript received 9 October 2014; published 20 November 2014)

We investigate the electronic structure of a perovskite-type Pauli paramagnet SrMoO₃ (t_{2g}^2) thin film using hard x-ray photoemission spectroscopy and compare the results to realistic calculations that combine density functional theory within the local-density approximation (LDA) with dynamical mean-field theory (DMFT). Despite the clear signature of electron correlations in the electronic specific heat, the narrowing of the quasiparticle bands is not observed in the photoemission spectrum. This is explained in terms of the characteristic effect of Hund's rule coupling for partially filled t_{2g} bands, which induces strong quasiparticle renormalization already for values of Hubbard interaction which are smaller than the bandwidth. This interpretation is supported by DMFT model calculations including Hund's rule coupling, which show a renormalization of low-energy quasiparticles without affecting the overall bandwidth. The photoemission spectra show additional spectral weight around -2.5 eV that is not present in the LDA+DMFT results, pointing to a source of correlations that is not present in our calculations that include only on-site interactions. We interpret this weight as a plasmon satellite, which is supported by the measured core-level spectra that all show satellites at this energy.

DOI: [10.1103/PhysRevB.90.205131](https://doi.org/10.1103/PhysRevB.90.205131)

PACS number(s): 71.30.+h, 71.28.+d, 73.61.-r, 79.60.Dp

I. INTRODUCTION

Electron correlations in transition-metal oxides (TMOs) have been the subject of extensive studies in recent decades [1]. Photoemission spectroscopy has made major contributions to a better understanding of electron correlation effects in those materials. The perovskite metallic compound SrVO₃ has been extensively studied as a prototypical correlated system with the t_{2g}^1 configuration and no magnetism [2,3]. The bulk spectrum of the V 3d bands of this compound was obtained by using soft x-ray (SX) photoemission spectroscopy, and it was found [4] that the width of the low-energy peak in the measured density of states (quasiparticle bandwidth) W^* is reduced to about half of that found in the band-structure calculation W_b , that is $W_b/W^* \sim 2$. This is consistent with specific-heat measurements, which suggest $m^*/m_b = \gamma/\gamma_b \sim 2$, where γ is the experimental specific heat coefficient, γ_b is the theoretical specific heat coefficient obtained from the band-structure calculations, m^* is the effective mass of the quasiparticle, and m_b is the bare band mass [5]. The photoemission spectra also displayed a clear lower Hubbard band at a binding energy ~ -1.5 eV. Such a photoemission signal with well-separated

Hubbard bands and a narrow quasiparticle peak has become an icon of correlated electron materials.

Surprisingly, the situation in TMOs with more than one d electron, and more extended orbitals (as found in the $4d$ transition-metal oxides), has been found to be quite different. Among such systems, SrRuO₃ (t_{2g}^4) has attracted particular interest due to its metallicity and ferromagnetism with $T_C \sim 160$ K [6]. Takizawa *et al.* [7] obtained a bulk Ru 4d spectrum of SrRuO₃ through SX photoemission studies of *in situ* prepared thin films, and found that the bandwidths obtained from the experimental bulk spectrum agree with those found in the band-structure calculation, that is, $W_b/W^* \sim 1$. This result, however, does not match with $m^*/m_b = \gamma/\gamma_b \sim 4$ found from specific heat measurements [8,9]. At this point however, it is important to emphasize that W^* denotes (here and in all the following) the width of the low-energy part of the spectral function as obtained from angle-integrated photoemission. Only a detailed study of quasiparticle dispersions and lifetimes from angle-resolved photoemission can resolve which part of this low-energy density of states is indeed associated with coherent quasiparticles, and which part is actually associated with more incoherent excitations.

In another t_{2g}^4 system Sr₂RuO₄, which is a layered superconductor [10], the situation is quite similar to SrRuO₃ in the sense that $W_b/W^* \sim 1$ but $m^*/m_b = \gamma/\gamma_b \sim 4$ [10–12]. These facts are summarized in Table I. The absence of pronounced Hubbard bands in the photoemission spectra of

*wadati@ap.t.u-tokyo.ac.jp; <http://www.geocities.jp/qxbqd097/index2.htm>

TABLE I. Effects of electron correlation in transition-metal oxides. The values of γ , γ/γ_b ($=m^*/m_b$), and W_b/W^* are given. The values without reference numbers are from this work.

	γ (mJ/K ² mol)	γ/γ_b ($=m^*/m_b$)	W_b/W^*
SrVO ₃ (t_{2g}^1)	8.182 ^a	$\sim 2^a$	$\sim 2^b$
SrRuO ₃ (t_{2g}^4)	36.3 ^c	$\sim 4^c$	$\sim 1^d$
Sr ₂ RuO ₄ (t_{2g}^4)	39 ^e	$\sim 4^f$	$\sim 1^g$
SrMoO ₃ (t_{2g}^2)	7.9 ^h	~ 2	~ 1

^aReference [5].

^bReference [4].

^cReference [9].

^dReference [7].

^eReference [10].

^fReference [11].

^gReference [12].

^hReference [19].

ruthenates led some of the researchers in the field to adopt the extreme view that electronic correlations are altogether absent or negligible in SrRuO₃ and CaRuO₃ compounds [13], which however, is incompatible with the measured enhancement of specific heat. Takizawa *et al.* [7] instead proposed that despite the absence of the Hubbard bands in the spectrum, only the states in the vicinity of the Fermi level (E_F) are to be thought of as originating from the genuinely coherent renormalized quasiparticle band, whereas the rest of the signal originates from the shorter lived states with bare dispersion. Very recently, theoretical studies within dynamical mean-field theory (DMFT) have indeed shown that Hund's rule coupling can (depending on the atomic occupancy) reduce the coherence energy scale already at moderate interaction strength [14,15] and that when this is the case, the Hubbard bands cannot be unambiguously resolved from an angle-integrated spectrum [16].

In the present work we reconsider these ideas and approach the problematics from two sides.

In the first purely theoretical part of the paper we report the correlated density of states (DOS) for a three-orbital problem with semicircular DOS for different strengths of the Hund's rule coupling and show explicitly how the Hubbard bands are being pulled in as the Hund's rule coupling strength increases. For physical values of Hund's rule coupling, most of the spectral weight is redistributed within the low-energy peak instead of being shifted to the Hubbard satellites as is the case in oxides with just an electron, such as SrVO₃. Similar results have been discussed earlier for iron-based superconductors [16].

In the second part of the paper we experimentally and theoretically study the correlated DOS of another perovskite-type $4d$ oxide SrMoO₃. Molybdates are particle-hole analogs of ruthenates as far as the occupancy of the t_{2g} shell is concerned: in SrMoO₃ ($4d^2$) the t_{2g} band is occupied by two electrons, and in SrRuO₃ (low-spin $4d^4$) the t_{2g} band is occupied by two holes. An advantage of SrMoO₃ is that it is a Pauli paramagnetic metal [17] and is therefore free from effects of proximity to magnetic instabilities that have been discussed

for ruthenates [18]. Nagai *et al.* [19] reported that SrMoO₃ single crystals grown in ultralow oxygen pressure have a resistivity as low as $5.1 \mu\Omega$ cm at 300 K. Recently Radetnac *et al.* [20] reported the fabrication of high-quality SrMoO₃ thin films using argon gas in the pulsed laser deposition (PLD) process. In this study we fabricated the same type of thin film which has atomic-level flatness at the surface (with a root-mean-square roughness of 0.2 nm [20]) and performed hard x-ray (HX) photoemission spectroscopy measurements. By applying bulk-sensitive HX photoemission spectroscopy to the atomically flat surface, we succeeded in obtaining the spectrum of bulk Mo $4d$ bands. Similarly to the case of SrRuO₃, the $4d$ peak in the photoemission does not appear to be narrowed with respect to the result of the LDA (i.e., $W^* \sim W_b$), despite the renormalized specific heat coefficient. Unlike in SrRuO₃, a pronounced shoulder at -2 eV is seen in our data.

We also performed realistic LDA+DMFT calculations of SrMoO₃. The low-energy part of the spectra is renormalized, consistent with the specific heat measurements, yet the overall band is not significantly narrowed. The additional spectral weight found experimentally at ~ -2 eV is however *not* present in our theoretical results. The failure of our theory to account for this weight points to electronic correlations that are not included in our approach. One possible explanation is that the -2 eV weight is a plasmonic satellite that originates in long range Coulomb interactions which are disregarded in our treatment. The satellites are seen in the measured core-level spectra, too. We note that SrMoO₃ is unique among transition metal oxides in the sense that it has a sizable gap with no LDA DOS in the -2 to -3.5 eV range, which is perhaps why these plasmonic effects are more seen here than they would be in another compound where they would overlap with the, e.g., oxygen states. We also note that extensions of the DMFT to include long range interactions have been developed, see, e.g., Refs. [21,22] and that it would be highly desirable to attempt to calculate the photoemission signal in SrMoO₃ properly incorporating the effects of long range interaction.

The paper is structured as follows. In Sec. II A we describe some details of the theoretical work, and in Sec. II B we describe the experimental procedure. Section III contains DMFT results for a model system that shows explicitly how Hubbard bands are pulled in by the Hund's rule coupling, which supports our interpretation of the experimental spectra. In Secs. IV A and IV B we report the photoemission results and compare them to what is found in the band-structure LDA and LDA+DMFT calculations. In Sec. IV C we give LDA+DMFT self-energies and discuss LDA+DMFT results in more details. Section V contains discussion of our results and conclusion.

II. DESCRIPTION OF THEORETICAL AND EXPERIMENTAL APPROACH

A. Theory

The DMFT model calculations and realistic LDA+DMFT calculations were done in the framework described in Refs. [23,24]. The DMFT model calculations were done using a semicircular density of states, with a full rotationally invariant Kanamori local interaction Hamiltonian.

For the realistic calculations, the band structure of SrMoO₃ was calculated using the linearized augmented plane wave method implemented in the WIEN2K package [25]. Bulk SrMoO₃ has an orthorhombic crystal structure below 150 K, a tetragonal one between 150 and 250 K, and cubic structure at temperatures above 250 K [26]. The degree of distortions away from cubic symmetry in this compound is small, and we found that the band structure of the compound is not influenced by distortions significantly. The results which we report below are for the cubic perovskite structure with the lattice constant $a = 3.976 \text{ \AA}$ [26]. A full rotationally invariant interaction with Kanamori parameters $U = 3.0 \text{ eV}$ and $J = 0.3 \text{ eV}$ has been used [27]. Using these parameters, the calculated mass enhancement is ~ 2 , consistent with experiment. The analytical continuations of the data to real frequencies were performed using the stochastic maximum entropy method [28].

B. Experiment

The SrMoO₃ thin film was grown in the (001) direction on a GdScO₃ (110) substrate [$(a = 5.482 \text{ \AA}, b = 5.742 \text{ \AA}, c = 7.926 \text{ \AA})$ for the orthorhombic lattice ($\bar{a} = 3.967 \text{ \AA}$ for a pseudocubic lattice definition)] by the PLD method. Since the lattice constant of the cubic SrMoO₃ is 3.976 \AA [26], a lattice mismatch between substrate and film is only -0.2% . The thickness of the thin film was about 70 nm. The details of the fabrication were described in Ref. [20].

HX photoemission measurements were carried out at BL-47XU of SPring-8. No surface cleaning was performed before the measurements. The HX photoemission spectra were recorded using a Scienta R-4000 electron energy analyzer with a total energy resolution of 300 meV at the photon energy of 7.94 keV. We also performed SX photoemission measurements at Photon Factory BL-2C to obtain the information about surface states. The SX photoemission spectra were recorded using a Scienta SES-2002 electron energy analyzer with a total energy resolution of 300 meV at the photon energy of 780 eV. The position of E_F was determined by measuring the spectra of gold which was in electrical contact with the sample. All the spectra were measured at room temperature.

III. MODEL DMFT RESULTS

To set the basis, it is convenient to start from the results of de'Medici *et al.* [14,15] who calculated the quasiparticle weight Z in t_{2g} systems by including the effects of Hund's rule coupling J . The results for t_{2g}^1 and t_{2g}^2 are reproduced in Fig. 1, where U is the on-site Coulomb interaction and D is the half bandwidth. There is a marked difference between the t_{2g}^1 and t_{2g}^2 systems. In the case of the t_{2g}^1 system, a nonzero J increases Z , whereas in the case of the t_{2g}^2, t_{2g}^4 systems a nonzero J rather decreases Z (except in the regime of large U/W). This means that in the latter case even a small value of $U/W \lesssim 1$ can lead to a suppressed Z at small energy scales. Materials that show strong correlations that originate from the Hund's coupling have been dubbed Hund's metals [29]. Because in a Hund's metal, so small values of U/W are sufficient to suppress Z , the high energy scales cannot be separated from the small energy scales in a clear way.

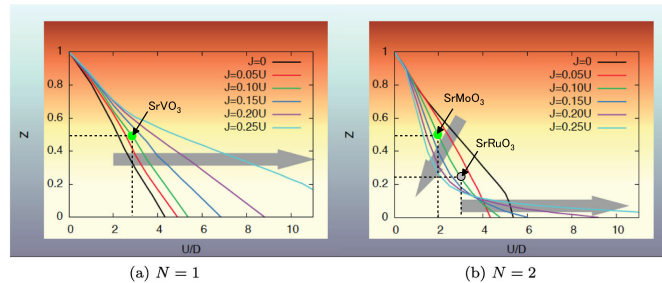


FIG. 1. (Color online) Quasiparticle weight Z as a function of U/D for $N = 1, 2$ electrons in three orbitals reproduced from Ref. [14]. The gray arrows indicate the influence of an increasing Hund's rule coupling J/U . Assuming $J/U = 0.1$, materials of interest to this study are positioned in the figure according to the measured specific heat enhancement. SrRuO₃, plotted in $N = 2$, is actually a d^4 occupancy and one should note that there is not an electron-hole symmetry for a t_{2g} DOS.

We calculated the momentum-integrated spectral function (DOS) for a three-orbital model with semicircular noninteracting DOS and a filling of two electrons per site, for several ratios of $J/U = 0.0, 0.05, 0.1, 0.15, 0.2$ (with $J/U = 0.15$ being close to the physical values for the transition-metal oxides). In order to ensure a fair comparison between these different cases, we adjusted U so that the low frequency mass renormalization remains the same: $m^*/m = Z^{-1} = 4$.

The calculated DOS are shown in Fig. 2. At $J/U = 0$, for sizable correlations to occur, the interaction strength must be tuned quite close to the Mott transition (which occurs for $U/D \approx 5.5$). The resulting spectra are akin to the spectra of metals close to a Mott insulator, displaying pronounced Hubbard bands and a narrow quasiparticle peak, implying a clear separation of high and low energy scales.

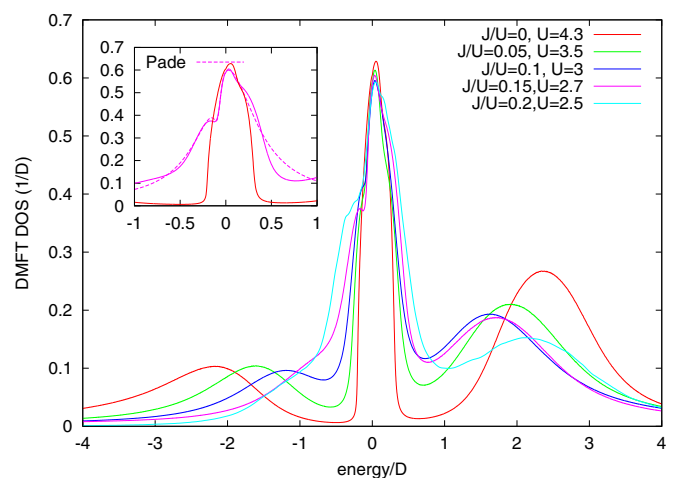


FIG. 2. (Color online) The DMFT DOS for a t_{2g} three-orbital model with semicircular noninteracting DOS occupied by two electrons per atom. Several values of J/U were used and U is adjusted so that the quasiparticle renormalization is close to $Z = 1/4$. Inset: Close-up on quasiparticle peak for $J/U = 0, 0.15$. For $J/U = 0.15$, also the Padé data are shown for comparison. Other curves are obtained using maximum entropy analytical continuation.

As J/U is increased, two effects occur [14,15]. First, as the correlations due to J develop, a smaller value of U is sufficient to reach the same degree of renormalization. Second, the effective atomic interaction for a transfer of electron [30], given by $E(N+1) + E(N-1) - 2E(N)$ that is equal to $U - 3J$ for a t_{2g} atom away from half-filling, is diminished even more with increasing J/U , thus the Hubbard bands are pulled in by the Hund's rule coupling J .

This is reflected in the spectra by the diminishing of the peak-to-peak distance between the Hubbard bands (4.7, 3.7, 2.7, 2.1 in units of D for increasing $J/U = 0.0, \dots, 0.15$, respectively—while the lower Hubbard band is essentially indistinguishable for $J/U = 0.2$). For $J/U = 0$ the peak is clearly separated from the atomic features and has a weight about 0.25, compatible with $Z = 0.25$. As J/U is increased, the coherent and incoherent excitations are not separated that clearly anymore. At $J/U = 0.15$, the lower Hubbard band starts to overlap with the quasiparticle band and remains visible only as a mild shoulder. The upper Hubbard band, however, remains visible. The high-energy and the low-energy scales are not separated, the incoherent spectral weight is transferred to energies which overlap with the quasiparticle band and therefore influence its shape. The quasiparticle peak appears broader and obtains an asymmetric shape. In the inset we replot the DOS on a narrower frequency range. The quasiparticle peak at $J/U = 0.15$ has a markedly different shape from that of the $J/U = 0$ case, whose shape resembles that of the narrowed noninteracting (semicircular) DOS. Next to the stochastic maximum entropy analytical continuation we show also the data obtained by the Padé approximants. The broadened quasiparticle peak with asymmetric shape and shoulder features at -0.2 eV is seen from both analytical continuations for $J/U = 0.15$. These features might be characteristic of Hund's metals and deserve further exploration.

In Fig. 3 we show the self-energies for $J/U = 0$ and $J/U = 0.15$. The real part of the self-energies exhibit sim-

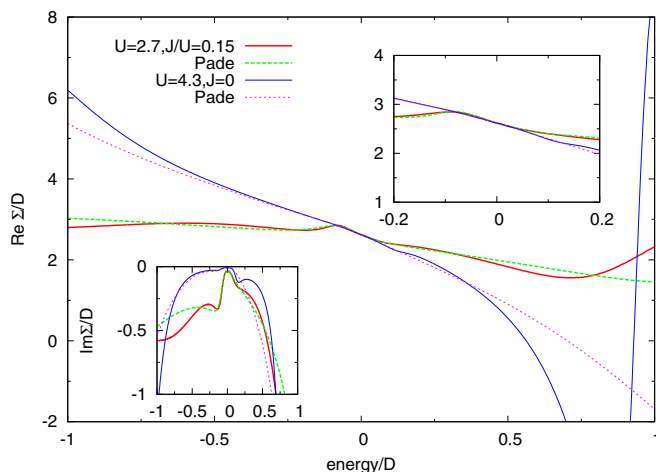


FIG. 3. (Color online) The DMFT self-energies for the t_{2g} three-orbital model for $J/U = 0$ and $J/U = 0.15$. Analytical continuations using Padé approximants and the maximum entropy method are shown. The $J/U = 0$ results are shifted vertically for easier comparison between the two data sets. Top inset: Close-up to low frequencies. Bottom inset: Imaginary part of self-energies.

ilar low frequency slope, which corresponds to the same quasiparticle residue Z , but in other aspects the data for $J/U = 0.15$ differ substantially from the data at vanishing Hund's coupling strength. The $J/U = 0$ real part of the self-energy follows a quasilinear dependence up to a high energy scale followed by an abrupt feature indicating the onset of the Hubbard band. Conversely, for $J/U = 0.15$ the real part of the self-energy is linear only up to a small frequency scale. At higher frequencies a relatively mild frequency dependence is seen, which indicates a weaker overall band narrowing. Except on approaching the Hubbard bands, the magnitude of $\text{Im}\Sigma$ (bottom inset) for $J/U = 0.15$ is larger, indicating correlations that develop due to the Hund's rule coupling despite a significantly smaller value of U . The genuine coherent, but strongly renormalized part, is thus actually limited to the low frequency scales ($\lesssim 0.1D$ for the present data), whereas at higher frequency scales a larger dispersion, but with much shorter lifetime is recovered.

Interesting further insight into the particular behavior of self-energies for Hund's metals is obtained by considering the Kramers-Kronig relations. Taking the following simple form: $\text{Im}\Sigma = -A\omega^2$ up to a cutoff ω_c , and $\text{Im}\Sigma = 0$ for $|\omega| > \omega_c$, we obtain from Kramers-Kronig relations: $\text{Re}\Sigma = -2\omega_c A\omega + \dots$. The slope of $\text{Re}\Sigma$ which determines the quasiparticle renormalization increases both with ω_c and A . At a fixed quasiparticle renormalization, this relation also shows that the cutoff frequency (which has the meaning of the energy of the kink) and the curvature are related. For vanishing Hund's rule coupling, the curvature of $\text{Im}\Sigma$ is small but persists up to a larger cutoff. For physical values of J , the curvature is larger, but it holds only up to a small frequency scale. This explains why in Hund's metals, like ruthenates, the kinks are often found (see, e.g., [31] and references therein) at small energy scales.

IV. PHOTOEMISSION AND LDA+DMFT RESULTS ON SrMoO_3

We now turn to SrMoO_3 , a metal with two electrons in conduction band that is therefore a possible realization of model results discussed above.

Below we first report photoemission results and later the comparison to the realistic LDA+DMFT calculations.

A. Photoemission results

Figure 4 shows the core-level photoemission spectra of the SrMoO_3 thin film. The O $1s$ spectrum [Fig. 4(a)] shows that the "contamination" signal on the higher binding-energy side is weak. The Sr $3d$ spectrum [Fig. 4(b)] has only one component at $3d_{5/2}$ and $3d_{3/2}$. These two results demonstrate that our photoemission spectra are free from surface degradation or contamination and represent the bulk electronic properties of the SrMoO_3 thin film. The Mo $3d$ spectrum [Fig. 4(c)] has two structures at -229.3 and -232.5 eV, almost the same as those of MoO_2 (Mo^{4+}) [32], representing the bulk Mo^{4+} states. This core level was also measured at 780 eV in the SX region, and two structures were observed at -233.3 and -236.4 eV, almost the same as those of MoO_3 (Mo^{6+}) [32]. It also has some weak Mo^{4+} signal at -229.3 eV. These results mean

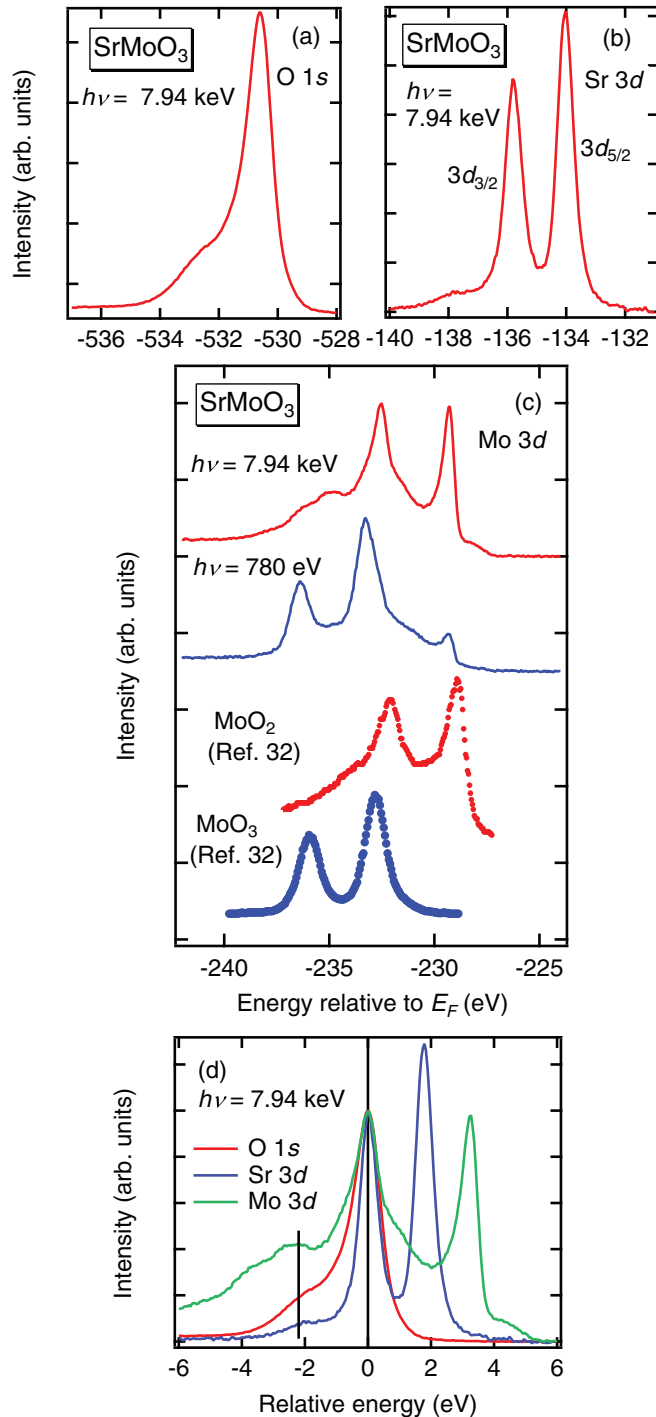


FIG. 4. (Color online) Core-level photoemission spectra of the SrMoO₃ thin film. (a) O 1s. (b) Sr 3d. (c) Mo 3d. The Mo 3d spectra were measured by both HX and SX, plotted together with the reference spectra of MoO₂ and MoO₃ [32]. (d) All the core levels plotted as a function of relative energy to the main peak.

that our thin film had Mo⁴⁺ in bulk and the surface states were dominated by Mo⁶⁺. Since Mo⁶⁺ has no 4d electrons, such surface oxidized states do not affect the Mo 4d band which will appear in subsequent figures.

There is also some additional intensity in all the core levels, that is, at -532.5 eV in O 1s [Fig. 4(a)], at -138 eV in

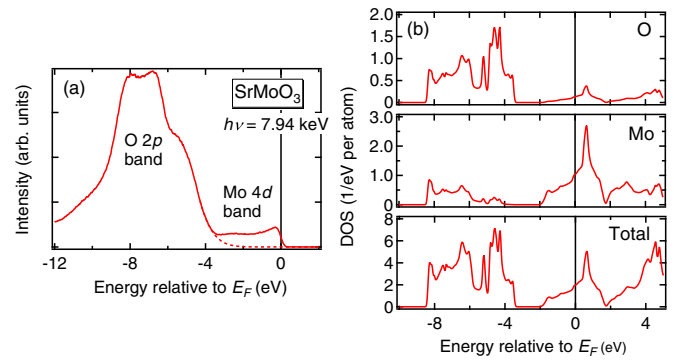


FIG. 5. (Color online) Electronic structure of SrMoO₃ near the Fermi level. (a) Valence-band photoemission spectrum of a SrMoO₃ thin film. The dashed line shows the estimated tail of the O 2p band. (b) The DOS of SrMoO₃ obtained from LDA band-structure calculations.

Sr 3d [Fig. 4(b)], and at -235 eV in Mo 3d [Fig. 4(c)]. We plotted these three core levels as a function of relative energy to the main peak in Fig. 4(d). One can see the intensity around -2 eV in all the core levels, which points to a common origin. As we discuss in more detail later, we believe that these structures are due to plasmon satellite. The energy of ~2 eV coincides closely with the plasma frequency reported in the measurements of reflectivity [33].

Figure 5(a) shows the valence-band photoemission spectrum of the SrMoO₃ thin film. By comparing the photoemission spectrum with the DOS deduced from the LDA [Fig. 5(b)], one can see that the Mo 4d band is located near E_F , and the O 2p band is located on the higher-energy side (from -4 to -10 eV). The dashed line in Fig. 5(a) shows the tail of the O 2p band extended towards the Mo 4d band. One can also clearly see the Mo 4d band crossing E_F and that the photoemission signal is described well by the LDA DOS, as further documented in Fig. 6.

B. Comparison of photoemission to LDA and LDA+DMFT

Figure 6(a) shows the bulk *d* orbital component obtained by subtracting the oxygen contribution [dashed line in Fig. 5(a)] from the photoemission signal. This photoemission DOS is compared to the results from the LDA band-structure calculation for SrMoO₃ as well as to the *t*_{2g} DOS from the LDA+DMFT calculation, which includes the effects of correlation. For the sake of comparison, results for SrVO₃ are also shown in Fig. 6(b), where the experimental spectrum is taken from Ref. [4]. The calculated DOS has been broadened with a Gaussian of 0.3 eV (FWHM: a full width at half maximum) and an energy-dependent Lorentzian (FWHM = 0.2|*E* - *E*_F| eV) [34] to account for the instrumental resolution and the lifetime broadening of the photohole, respectively. The theoretical data were multiplied by the Fermi function. Bare theoretical data are presented in Sec. IV C.

The first observation is that the experimental photoemission is distinct from the LDA results, which is a signature of electronic correlations. In the case of SrVO₃, these manifest in a well-known way: the quasiparticle band is narrowed and a split-off lower Hubbard band is seen. These results are reproduced very well by the LDA+DMFT.

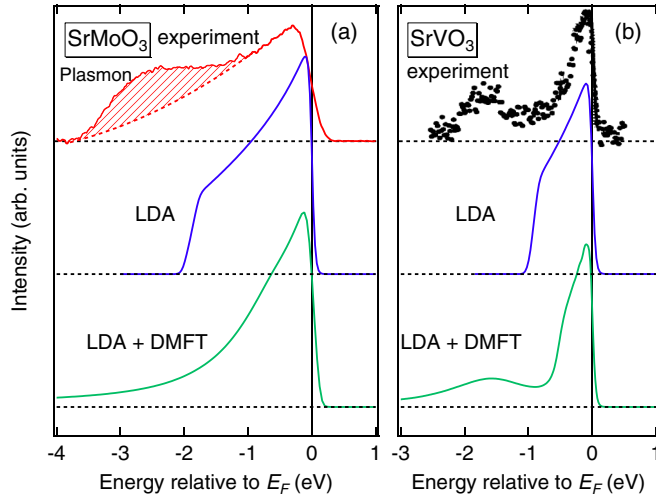


FIG. 6. (Color online) Comparison of the bulk component obtained by photoemission spectroscopy and the band-structure calculation for SrMoO₃ (a) and SrVO₃ (b). The experimental spectrum of SrVO₃ is from Ref. [4]. The calculated DOS has been broadened with a Gaussian and a Lorentzian function. The hump structure at -2.5 eV in experiment (a) is attributed to a plasmon satellite.

In the case of SrMoO₃, the electronic correlations manifest in a different way. The observed photoemission does not show band narrowing. Rather, the quasiparticle band appears to be widened and develops a hump at energy -2.5 eV.

Interestingly, in the LDA+DMFT results, although part of the spectral weight extends to frequencies below -2 eV due to the large imaginary part of the self-energy found in this energy range (reported below), the pronounced hump found experimentally at ~ -2.5 eV is not found. This leads us to propose that the hump is not a Hubbard band. Note also that the hump occurs at an energy which is separated more from the Fermi energy than the Hubbard band in SrVO₃, whereas the interaction parameters are expected to be smaller for $4d$ elements than for $3d$ elements due to the more extended orbitals of the former. This is also consistent with the comparison made in Ref. [13] between the photoemission spectra and first-principles calculations of $4d$ TMOs CaRuO₃ and SrRuO₃ vs $3d$ TMOs.

What is then the origin of the hump? Whereas more work will be needed to clarify this conclusively, we believe the most natural explanation is that it is a plasmon satellite. The plasma edge in the optical experiments [33] is indeed at about 2 eV, and we stress again that the satellite structures are seen also in all the core levels. Influence of plasmons in core-level photoemission spectra was observed in simple metals like Mg [35,36] and conducting oxides like Na_xWO₃ [37] and K_{0.3}MoO₃ [38]. In correlated materials the influence of plasmons on photoemission is discussed less often. We note that the plasma frequencies are about 2 eV, which means that they often overlap with the Hubbard band and that therefore $4d$ oxides that do not show pronounced Hubbard bands might be promising materials to investigate plasmons further. Molybdates, that have a gap in the LDA spectrum between -3 and -2 eV, are particularly promising in this respect.

C. LDA+DMFT DOS and self-energies

For SrVO₃ the values of interaction $U = 4.5$ eV and $J/U = 0.15$ were used in the calculation. Note that the calculations performed here involve only the t_{2g} states. Hence these values of the interaction parameters should be understood as low-energy values taking into account the screening from all other bands. Starting from the same ratio of atomic interaction parameters $J_{\text{atom}}/U_{\text{atom}}$ the screened values of J/U can be expected to be higher in $3d$ oxides, because the screening which is stronger in $3d$ oxides due to the proximity of the oxygen states affects more U than the J which is related to higher orders of the multipole expansion of the Coulomb interaction.

In the top panels of Fig. 7 the LDA+DMFT DOS are compared to the LDA DOS for SrMoO₃ (data shown left) and SrVO₃ (right). In the case of SrVO₃, $U/W \sim 2 > 1$, leading to a split-off lower Hubbard band. In contrast, for SrMoO₃ one has $U/W \lesssim 1$, hence the high energy features are merged with the quasiparticle band. More pronounced difference as well as a precursor of the Hubbard band at about 1.5 eV are actually found on the positive frequency side which is not accessible to photoemission experiments.

In the middle panels of Fig. 7 we display the real part of the real-frequency self-energy $\Sigma(\omega)$, and in the bottom panels its imaginary part. For SrMoO₃, on the negative energy side, the self-energy deviates from the linear behavior at about -0.5 eV (kink, signaled by an arrow). At larger binding energy, it levels

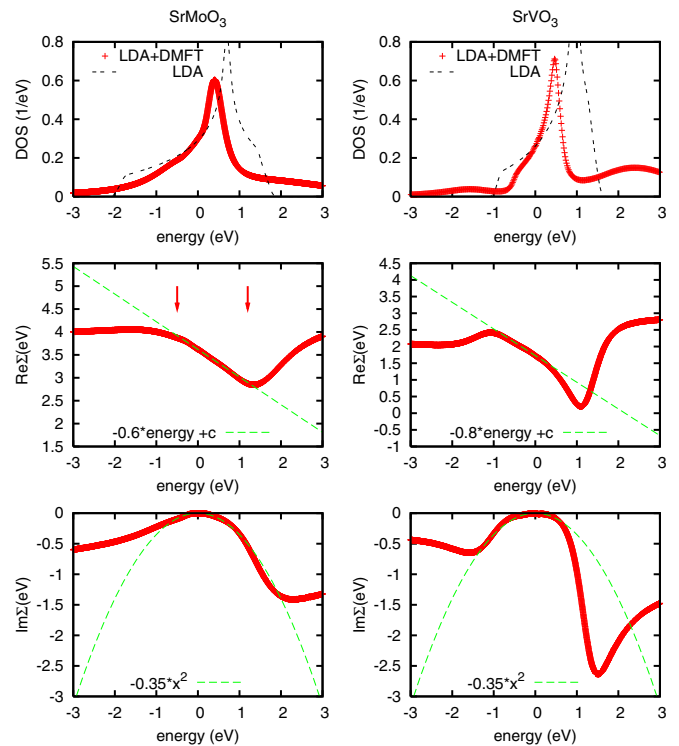


FIG. 7. (Color online) Top panels: LDA and LDA+DMFT DOS for SrMoO₃ (left) and SrVO₃ (right). Medium panels: Real parts of self-energy. The dashed lines are fits to the low-energy linear behavior. Departure from this behavior is indicated by arrows, associated with kinks in the dispersion of electronic excitations. Bottom panels: Imaginary parts of the self-energy, with corresponding quadratic fit to the low-energy (Fermi liquid) behavior.

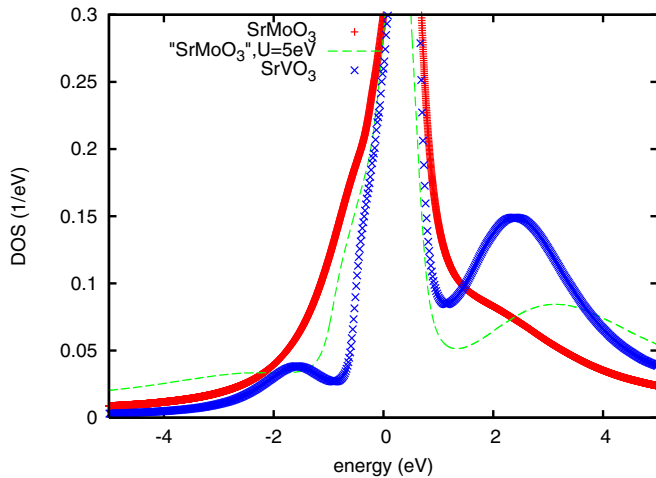


FIG. 8. (Color online) LDA+DMFT DOS for SrMoO_3 and SrVO_3 . For SrMoO_3 also the data for unphysically large $U = 5$ eV are shown.

off to a frequency-independent behavior, recovering the bare LDA dispersion, although with significant broadening (as clear from $\text{Im}\Sigma$, shown in the lower panel). In contrast, for SrVO_3 the imaginary part of the self-energy displays a weak polelike structure, signaling the Hubbard band, and a related feature with positive slope in the real part of the self-energy in the same energy range.

The magnitude of $\text{Im}\Sigma$ is found to be comparable at small frequencies (note that the data are described well by a parabola with similar curvature for both materials). At higher frequencies ~ 1 eV, on the other hand, the magnitude of $\text{Im}\Sigma$ in SrMoO_3 becomes relatively smaller, which is another manifestation of the fact that the electronic correlations originate from the Hund's rule induced multiplet splitting which become unimportant at frequencies above J .

As the fate of the lower Hubbard band in SrMoO_3 is important for the interpretation of our experimental results, we tuned the interaction values also to larger values. For SrMoO_3 one needs to increase U to $U = 5$ eV (keeping $J = 0.3$ eV) for the split-off lower Hubbard band to start showing up. This value is unphysically large for a screened t_{2g} interaction associated with a transition-metal oxide of the $4d$ series. The data are displayed in Fig. 8, next to the data for SrMoO_3 and SrVO_3 at physical interaction strengths. The scale is adjusted so that the satellites are most visible. The data at $U \sim 5$ eV would describe the experimental photoemission but the mass enhancement is larger ~ 2.6 , which is inconsistent with the specific heat measurements.

V. CONCLUSION

We have studied the electronic structures of a SrMoO_3 thin film by HX photoemission spectroscopy. From the Mo $3d$ core level, we found that the valence of Mo is indeed $4+$ in the bulk. The valence-band spectrum clearly showed the Mo $4d$ band crossing E_F .

The obtained bulk Mo $4d$ spectra do not appear to be narrower than the ones calculated from band theory within

the LDA approximation which is at odds with the measured electronic specific-heat coefficient that is about twice larger than the band value. The spectra show an additional spectral weight at -2 eV.

We performed theoretical model calculations within DMFT. In the presence of Hund's rule coupling these exhibit renormalizations followed by kinks that occur at a small energy. At energies above the kink energy, the bare dispersions are recovered, which reconciles absence of overall band narrowing with the specific heat enhancement. Taking these results together suggest that only the low energy part of the SrMoO_3 spectra near E_F comes from genuinely coherent quasiparticle states. Such a behavior was also observed in SrRuO_3 .

We also performed realistic LDA+DMFT calculations of SrMoO_3 . Interestingly, these did not account for the broad hump at ~ -2.5 eV observed in the photoemission spectrum. The relatively high-binding energy of this feature, as well as the discrepancy with LDA+DMFT suggest that this hump is not a lower Hubbard band. We suggest that it is a plasmon satellite and propose that molybdates might be an interesting material to investigate the physics of plasmons in correlated materials further.

Future studies using angle-resolved photoemission are especially desirable. Indeed, it should then be possible to distinguish between the truly coherent part of the low-energy spectrum corresponding to quasiparticles with a reduced velocity, and the higher energy excitations which both contribute to the observed angle-integrated photoemission signal within ~ -1 eV of the Fermi level. Furthermore, our theoretical calculations predict a kink in the electronic dispersion at about -0.5 eV, signaling the crossover between these two types of excitations. As recently discussed in Ref. [39] for Sr_2RuO_4 , these abrupt changes of the electronic dispersion on the negative—as well as on the positive—energy side of the spectrum may lead to observable signatures in optical spectroscopy. Angle-resolved photoemission study will also be helpful in discriminating if the -2 eV hump is indeed a plasmon, as we propose here.

ACKNOWLEDGMENTS

This research was granted by the Japan Society for the Promotion of Science (JSPS) through the "Funding Program for World-Leading Innovative R&D on Science and Technology (FIRST Program)," initiated by the Council for Science and Technology Policy (CSTP). This work was supported in part by JSPS Grant-in-Aid for Scientific Research(S) No. 24224009. The synchrotron radiation experiments at SPring-8 were performed under the approval of the Japan Synchrotron Radiation Research Institute (2010B1740 and 2011A1624). The synchrotron radiation experiments at KEK-PF were performed under the approval of the Program Advisory Committee (Proposal No. 2008S2-003) at the Institute of Materials Structure Science, K.E.K. The computing time was provided by IDRIS-GENCI under Grant 2011091393. J.M. acknowledges support of the Slovenian Research Agency (ARRS) under Program P1-0044 and A.G. the support of the European Research Council (Grant ERC-319286 QMAC).

- [1] M. Imada, A. Fujimori, and Y. Tokura, *Rev. Mod. Phys.* **70**, 1039 (1998).
- [2] A. Fujimori, I. Hase, H. Namatame, Y. Fujishima, Y. Tokura, H. Eisaki, S. Uchida, K. Takegahara, and F. M. F. de Groot, *Phys. Rev. Lett.* **69**, 1796 (1992).
- [3] I. H. Inoue, I. Hase, Y. Aiura, A. Fujimori, Y. Haruyama, T. Maruyama, and Y. Nishihara, *Phys. Rev. Lett.* **74**, 2539 (1995).
- [4] A. Sekiyama, H. Fujiwara, S. Imada, S. Suga, H. Eisaki, S. I. Uchida, K. Takegahara, H. Harima, Y. Saitoh, I. A. Nekrasov, G. Keller, D. E. Kondakov, A. V. Kozhevnikov, T. Pruschke, K. Held, D. Vollhardt, and V. I. Anisimov, *Phys. Rev. Lett.* **93**, 156402 (2004).
- [5] I. H. Inoue, O. Goto, H. Makino, N. E. Hussey, and M. Ishikawa, *Phys. Rev. B* **58**, 4372 (1998).
- [6] A. Callaghan, C. W. Moeller, and R. Ward, *Inorg. Chem.* **5**, 1572 (1966).
- [7] M. Takizawa, D. Toyota, H. Wadati, A. Chikamatsu, H. Kumigashira, A. Fujimori, M. Oshima, Z. Fang, M. Lippmaa, M. Kawasaki, and H. Koinuma, *Phys. Rev. B* **72**, 060404(R) (2005).
- [8] P. B. Allen, H. Berger, O. Chauvet, L. Forro, T. Jarlborg, A. Junod, B. Revaz, and G. Santi, *Phys. Rev. B* **53**, 4393 (1996).
- [9] J. Okamoto, T. Mizokawa, A. Fujimori, I. Hase, M. Nohara, H. Takagi, Y. Takeda, and M. Takano, *Phys. Rev. B* **60**, 2281 (1999).
- [10] Y. Maeno, H. Hashimoto, K. Yoshida, S. Nishizaki, T. Fujita, J. G. Bednorz, and F. Lichtenberg, *Nature (London)* **372**, 532 (1994).
- [11] T. Oguchi, *Phys. Rev. B* **51**, 1385 (1995).
- [12] Z. V. Pchelkina, I. A. Nekrasov, T. Pruschke, A. Sekiyama, S. Suga, V. I. Anisimov, and D. Vollhardt, *Phys. Rev. B* **75**, 035122 (2007).
- [13] K. Maiti and R. S. Singh, *Phys. Rev. B* **71**, 161102 (2005).
- [14] L. de' Medici, J. Mravlje, and A. Georges, *Phys. Rev. Lett.* **107**, 256401 (2011).
- [15] A. Georges, L. de' Medici, and J. Mravlje, *Annu. Rev. Condens. Matter Phys.* **4**, 137 (2013).
- [16] A. Kutepov, K. Haule, S. Y. Savrasov, and G. Kotliar, *Phys. Rev. B* **82**, 045105 (2010).
- [17] G. H. Bouchard and M. J. Sienko, *Inorg. Chem.* **7**, 441 (1968).
- [18] G. Cao, W. Song, Y. Sun, and X. Lin, *Solid State Commun.* **131**, 331 (2004).
- [19] I. Nagai, N. Shirakawa, S. Ikeda, R. Iwasaki, H. Nishimura, and M. Kosaka, *Appl. Phys. Lett.* **87**, 024105 (2005).
- [20] A. Radetinac, K. S. Takahashi, L. Alff, M. Kawasaki, and Y. Tokura, *Appl. Phys. Express* **3**, 073003 (2010).
- [21] P. Hansmann, T. Ayrál, L. Vaugier, P. Werner, and S. Biermann, *Phys. Rev. Lett.* **110**, 166401 (2013).
- [22] L. Huang, T. Ayrál, S. Biermann, and P. Werner, *Phys. Rev. B* **90**, 195114 (2014).
- [23] M. Aichhorn, L. Pourovskii, V. Vildosola, M. Ferrero, O. Parcollet, T. Miyake, A. Georges, and S. Biermann, *Phys. Rev. B* **80**, 085101 (2009).
- [24] M. Ferrero and O. Parcollet, TRIQS: <http://ipht.cea.fr/triqs>.
- [25] P. Blaha, K. Schwarz, G. Madsen, D. Kvasnicka, and J. Lutz, *WIEN2k, An Augmented Plane Wave + Local Orbitals Program for Calculating Crystal Properties* (Techn. Universitat Wien, Austria, 2001).
- [26] R. B. Macquart, B. J. Kennedy, and M. Avdeev, *J. Solid State Chem.* **183**, 250 (2010).
- [27] L. Vaugier, H. Jiang, and S. Biermann, *Phys. Rev. B* **86**, 165105 (2012).
- [28] K. S. D. Beach, [arXiv:cond-mat/0403055](https://arxiv.org/abs/cond-mat/0403055).
- [29] Z. P. Yin, K. Haule, and G. Kotliar, *Nat. Mater.* **10**, 932 (2011).
- [30] L. de' Medici, *Phys. Rev. B* **83**, 205112 (2011).
- [31] J. Mravlje, M. Aichhorn, T. Miyake, K. Haule, G. Kotliar, and A. Georges, *Phys. Rev. Lett.* **106**, 096401 (2011).
- [32] R. J. Colton, A. M. Guzman, and J. W. Rabalais, *J. Appl. Phys.* **49**, 409 (1978).
- [33] H. Mizoguchi, N. Kitamura, K. Fukumi, T. Mihara, J. Nishii, M. Nakamura, N. Kikuchi, H. Hosono, and H. Kawazoe, *J. Appl. Phys.* **87**, 4617 (2000).
- [34] H. Höchst, P. Steiner, G. Reiter, and S. Hüfner, *Z. Phys. B* **42**, 199 (1981).
- [35] L. Ley, F. R. McFeely, S. P. Kowalczyk, J. G. Jenkin, and D. A. Shirley, *Phys. Rev. B* **11**, 600 (1975).
- [36] L. Ley and M. Cardona, *Photoemission in Solids II* (Springer, Berlin, 1979).
- [37] J.-N. Chazalviel, M. Campagna, G. K. Wertheim, and H. R. Shanks, *Phys. Rev. B* **16**, 697 (1977).
- [38] G. K. Wertheim, L. F. Schneemeyer, and D. N. E. Buchanan, *Phys. Rev. B* **32**, 3568 (1985).
- [39] D. Stricker, J. Mravlje, C. Berthod, R. Fittipaldi, A. Vecchione, A. Georges, and D. van der Marel, *Phys. Rev. Lett.* **113**, 087404 (2014).